The Journal of Chemical Physics

Conical intersection seams in spin–orbit coupled systems with an even number of electrons: A numerical study based on neural network fit surfaces

Cite as: J. Chem. Phys. **155**, 174115 (2021); https://doi.org/10.1063/5.0067660
Submitted: 18 August 2021 • Accepted: 15 October 2021 • Published Online: 03 November 2021

Yuchen Wang and David R. Yarkony

The Journal of Chemical Physics ARTICLE scitation.org/journal/jcp

Conical intersection seams in spin–orbit coupled systems with an even number of electrons: A numerical study based on neural network fit surfaces

Cite as: J. Chem. Phys. 155, 174115 (2021); doi: 10.1063/5.0067660
Submitted: 18 August 2021 • Accepted: 15 October 2021 •
Published Online: 3 November 2021

Yuchen Wang[a] and David R. Yarkony[a]

AFFILIATIONS

Department of Chemistry, Johns Hopkins University, Baltimore, Maryland 21218, USA

[a]Authors to whom correspondence should be addressed: ywang312@jhu.edu and yarkony@jhu.edu

ABSTRACT

In this work, we consider the existence and topography of seams of conical intersections (CIs) for two key singlet–triplet systems, including a uniformly scaled spin–orbit interaction. The basic one triplet and one singlet state system denoted as (S_0,T_1) and the two singlets and one triplet system denoted as (S_0,S_1,T_1) are treated. Essential to this analysis are realistic electronic structure data taken from a recently reported neural network fit for the $1,2^1A$ and 1^3A states of NH_3, including H_{sf} (spin-free) and H_{so} (spin–orbit) surfaces derived from high quality *ab initio* wavefunctions. Three types of seams for the (S_0,S_1,T_1) system are reported, which depend on the choice of the electronic Hamiltonian, H^e. The nonrelativistic CI seam [$H^e = H_{sf}$, (S_0,S_1)], the energy minimized nonrelativistic singlet–triplet intersection seam [$H^e = H_{sf}$, (S_0,T_1)], and the fully relativistic seam in the spin-diabatic representation ($H^e = H_{tot} = H_{sf} + H_{so}$) are reported as functions of R(N–H). The derivative couplings are computed using $H^e = H_{tot}$ and H_{sf} from the fit data. The line integral of the derivative coupling is employed to juxtapose the geometric phase in the relativistic, $H^e = H_{tot}$, and nonrelativistic, $H^e = H_{sf}$, cases. It is found for the (S_0,T_1) system that there is no CI in the spin-adiabatic representation, while for the (S_0,S_1,T_1) system, CI can only be formed for two pairs of spin-adiabatic electronic states. The geometric phase effect thus needs to be handled with care when it comes to spin-nonconserving dynamics simulations.

I. INTRODUCTION

In electronically nonadiabatic processes, distinct adiabatic potential energy surfaces can intersect along a seam with the topology of a double cone known as a conical intersection (CI).[1–4] One extensively studied nonadiabatic process, internal conversion (IC), is a spin-conserving transition of the molecule from one electronic state to another. CIs are key to understanding internal conversion behavior as they serve as efficient funnels that transfer population between states.[5–10] Nonadiabatic behavior near a CI can be captured in an on-the-fly approach[11–13] or with the help of quasi-diabatic coupled potential energy surfaces.[9,10,14–16]

In the nonrelativistic case (Coulomb electronic Hamiltonian), CIs induce the geometric or Berry phase in which a real-valued electronic wavefunction changes sign when traversing along a closed loop that encloses an odd number of CIs.[17–20] The sign change renders the adiabatic electronic wavefunction double-valued. This double-valuedness needs to be removed from the total wavefunction by a geometry-dependent phase factor. It has been shown that the geometric phase (GP) effect can influence the multistate reaction dynamics significantly.[21–24] In a recent study, it was reported that dynamics on the single lower adiabatic surface and the influence of the GP effect are nontrivial, and excluding it can produce catastrophic results in adiabatic quantum dynamics.[25]

The above discussion focuses on CIs for spin conserving processes. However, recently, much work has been done[11,12,26–30] to include spin–orbit coupling in the electronic Hamiltonian, using on-the-fly techniques, to enable simulations of the spin-nonconserving process intersystem crossing (ISC), a process of interest in photochemistry and photobiology.[31–33] The principal difference between IC and ISC is that IC is spin-conserving, while ISC is not. Transitions between states with different spin multiplicities open new reaction pathways that may compete with IC.

IC can be treated either on-the-fly or with predetermined coupled fit surfaces. On-the-fly dynamics facilitates incorporation of the spin–orbit interaction into the spin-diabatic approximation since

the adiabatic electronic wavefunctions, solution to the electronic Schrödinger equation, are available at all time steps. For fit surface driven dynamics, the required spin–orbit coupling (or other properties) matrix elements are made available as functional forms, fit to the adiabatic *ab initio* data. This requires smooth data throughout the range of the fit. Adiabatic representations are not smooth near a conical intersection, where the derivative coupling is singular, and the GP must be considered. The discontinuity in the wavefunction affects wavefunction-based matrix elements. For example, the switching of wavefunction on a path that goes through a CI creates an artificial discontinuity in properties such as electronic dipole moments and spin–orbit coupling.[34,35] This discontinuity prevents the property from being fit with smooth functions over the entire nuclear coordinate space. A numerically better-behaved representation is the diabatic representation, which is related to the adiabatic representation by a unitary transformation (the AtD transformation; see below). In the diabatic representation, there is no singularity in derivative coupling as they are all zero. Unfortunately, strict diabatic states do not exist for molecules with three or more atoms; hence, although "quasi-diabatic" is a more precise expression for what we do here, we will drop the qualifier "quasi" for simplicity.[36] The diabatic representation renders the dipoles and spin–orbit coupling (SOC) matrix elements continuous functions of nuclear coordinates and can be readily fit by robust machine learning methods such as artificial neural networks (NNs).[37–39] This enables formulation of nonadiabatic dynamics codes to treat ISC based on accurate fit *ab initio* data.

In this work, using previously reported data, the (relativistic) spin–orbit interaction, in the Breit–Pauli approximation,[40,41] is incorporated into a spin conserving nonadiabatic Hamiltonian in the commonly used spin-diabatic representation (defined below), producing the spin nonconserving fully coupled potential energy surfaces to be used in the dynamics. Here, the treatment will be limited to systems with even numbers of electrons. The restriction to systems with an even number of electrons allows time reversal symmetry to be used to make all the Hamiltonian matrix elements real-valued[42] as they are in the nonrelativistic case. See Appendix A for a brief discussion of time reversal symmetry. Working in this fully coupled state space, analytic and numerical tools are used to demonstrate (for the first time) the existence of non-intuitive (see Sec. III) CI seams in the relativistic system, which are located, and their topographies are analyzed. Line integrals of derivative couplings along prescribed paths will describe the GP effect and help locate CIs. Our numerical analysis is enabled by neural network (NN) fit coupled potential energy surfaces and NN fits of spin–orbit coupling (SOC) data.[43]

This work is organized as follows. In Sec. II, we introduce the requisite electronic Hamiltonian, $H_{tot} = H_{sf} + H_{so}$, where H_{sf} is the spin-free nonrelativistic Hamiltonian and H_{so} describes the spin–orbit coupling. Note that the derivative coupling operator d/dR is spin-free, which renders our bases spin diabatic. Two systems will be treated, (S_0,T_1) being a generic "singlet–triplet" intersection with all components of the triplet included and (S_0,S_1,T_1), which describes a singlet conical intersection perturbed by a nearby triplet. Also described is the scaling of H_{so} used to emphasize its effects. The numerical analysis carried out here is enabled by the fact that the electronic structure data (ESD) including those obtained for H_{so} are available from fit functions. The fit data can be used to obtain, for example, the derivative couplings of H_{tot}, the (total) relativistic Hamiltonian (a key quantity; see below) by a divided difference with little computational effort. Section III presents the numerical results with emphasis on how the presence of the triplet and SOC impacts the conical intersection seam of the two fundamental nonadiabatic topographies, which have been studied previously in a surface hopping context.[44] Our analysis makes use of the circulation of the derivative coupling to confirm the existence of CI, an approach espoused and successfully implemented for nonrelativistic wavefunctions by Baer.[45–47] Section IV summarizes and discusses directions for future studies.

II. ELECTRONIC HAMILTONIANS AND DERIVED QUANTITIES

A. Two electronic Hamiltonians

The Hamiltonian studied in this work has the following form:

$$\mathbf{H}_{tot} = \mathbf{H}_{sf} + \mathbf{H}_{so}. \tag{1}$$

Here, $\mathbf{H}_{sf}$ is the spin-free part. $\mathbf{H}_{so}$ is the spin–orbit coupling term. The spin-free Hamiltonian satisfies the electronic Schrödinger equation

$$\left[\mathbf{H}_x^{(d)}(\mathbf{R}) - \mathbf{I}E_I^{(a)}(\mathbf{R})\right]\mathbf{d}^I(\mathbf{R}) = 0. \tag{2}$$

Here, (a), (d) denote the adiabatic and diabatic representation, $\mathbf{R}$ denotes the nuclear coordinates, and x = sf. $\mathbf{H}_{sf}^{(d)}$ is the model (nonrelativistic) diabatic Hamiltonian, which is an $N^{state} \times N^{state}$ matrix that is fit to the *ab initio* ESD (energy, energy gradients, and derivative coupling).

The derivative coupling between states with the same multiplicity can be obtained from *ab initio* calculations or the model Hamiltonian. For a detailed discussion on obtaining it through *ab initio* methods such as multireference configuration interaction (MRCI), we refer the reader to Ref. 48. In the fit model Hamiltonian, the basis is assumed diabatic and the adiabatic derivative coupling is evaluated with the following equation when $E_I^a(\mathbf{R}) \neq E_J^a(\mathbf{R})$:

$$\mathbf{f}_{IJ}^a = \left\langle \Psi_I^a(\mathbf{q},\mathbf{R}) | \nabla_R \Psi_J^a(\mathbf{q},\mathbf{R}) \right\rangle \approx \frac{\mathbf{d}^I(\mathbf{R})^\dagger (\nabla_R \mathbf{H}_x) \mathbf{d}^J(\mathbf{R})}{E_I^a(\mathbf{R}) - E_J^a(\mathbf{R})}. \tag{3}$$

The derivative coupling obtained using Eq. (3) is not restricted to x = sf, that is, states with the same multiplicity in Eq. (2). All that is required is that $\mathbf{H}_x$ used in Eq. (2) be the same as that used in Eq. (3). Considering a multistate system with singlets and triplets, I, J can represent states composed of linear combinations of triplet and singlet components. The gradients of $\mathbf{H}_x$ that appear in Eq. (3) can be determined by divided differences from the fit model Hamiltonian.

We now turn to the two practical examples introduced in Sec. I, the system (S_0,T_1) one singlet and one triplet. The total Hamiltonian

has the form of a 4 × 4 matrix,

$$\begin{array}{ccccc} H & |S_0\rangle & |T_1\rangle & |T_0\rangle & |T_{-1}\rangle \\ \langle S_0| & E_s & B_0 - iA_0 & iC_0 & B_0 + iA_0 \\ \langle T_1| & B_0 + iA_0 & E_t & 0 & 0 \\ \langle T_0| & -iC_0 & 0 & E_t & 0 \\ \langle T_{-1}| & B_0 - iA_0 & 0 & 0 & E_t \end{array} \tag{4}$$

Here, E_s is the H_{sf} determined electronic energy of the singlet and E_t is the electronic energy of the triplet. It is convenient to transform the triplet wavefunction to the following time reversal adapted basis:

$$\begin{aligned} |T_+^{tr}\rangle &= (|T_1\rangle + |T_{-1}\rangle)/\sqrt{2}, \\ |T_-^{tr}\rangle &= i(|T_1\rangle - |T_{-1}\rangle)/\sqrt{2}, \\ |T_0^{tr}\rangle &= -i|T_0\rangle. \end{aligned} \tag{5}$$

Here, the superscript tr (suppressed below) denotes the time reversal basis. The SOC matrix elements will be real using a time reversal basis.[42] While this is a significant simplification, dealing with the complex matrix is possible[11] but will not be discussed here. Define $X_j = \sqrt{2}A_j$, $Y_j = \sqrt{2}B_j$, and $Z_j = C_j$ (j = 0, 1); the Hamiltonian matrix then becomes

$$\begin{array}{ccccc} H & |S_0\rangle & |T_-\rangle & |T_+\rangle & |T_0\rangle \\ \langle S_0| & E_s & X_0 & Y_0 & Z_0 \\ \langle T_-| & X_0 & E_t & 0 & 0 \\ \langle T_+| & Y_0 & 0 & E_t & 0 \\ \langle T_0| & Z_0 & 0 & 0 & E_t \end{array} \tag{6}$$

The representation is called the spin-diabatic representation[44] since there is no derivative coupling between functions with different S, M_S values. For dynamics purposes, one should expect such representations to be smooth over the entire accessible nuclear coordinate space.

By diagonalizing (6), we obtained the spin-adiabatic representation.[44] It is clear that the triplets in the spin-adiabatic representation are no longer threefold degenerate. In fact, one can write down the following eigenvalues:

$$\begin{aligned} \lambda_2 &= E_t, \\ \lambda_3 &= E_t, \\ \lambda_1 &= \frac{1}{2}\left(E_s + E_t - \sqrt{(E_s - E_t)^2 + 4(X_0^2 + Y_0^2 + Z_0^2)}\right), \\ \lambda_4 &= \frac{1}{2}\left(E_s + E_t + \sqrt{(E_s - E_t)^2 + 4(X_0^2 + Y_0^2 + Z_0^2)}\right), \end{aligned} \tag{7}$$

clearly evincing a double degeneracy in the spin-adiabatic representation. Moreover, requiring $\lambda_1 = E_t$ or $\lambda_4 = E_t$ will give $X_0^2 + Y_0^2 + Z_0^2 = 0$. This means that the system will exhibit an unexpected four state degeneracy in the N − 4 dimensional subspace in which $E_t = E_s$ and $X_0 = Y_0 = Z_0 = 0$, an occurrence that is expected to be rare.

We next examine the system with two singlets S_0, S_1 and one triplet T_1. Since S_0 and S_1 are coupled adiabatic states with a seam of CIs in the nonrelativistic case, before introducing the SOC term to the total Hamiltonian, one needs to use a suitable diabatization technique to diabatize the singlets and transform the spin–orbit coupling to that representation, making it smooth.

For a two state diabatization, the adiabatic to diabatic transformation reads

$$\begin{pmatrix} |S_0^d\rangle \\ |S_1^d\rangle \end{pmatrix} = \begin{pmatrix} \cos\theta & -\sin\theta \\ \sin\theta & \cos\theta \end{pmatrix} \begin{pmatrix} |S_0^a\rangle \\ |S_1^a\rangle \end{pmatrix}. \tag{8}$$

In previous papers, we have shown that the adiabatic spin–orbit coupling obtained from standard quantum chemistry packages is not continuous in the vicinity of CIs due to the rapid switching of adiabatic electronic wavefunctions in this region.[35] To remove the discontinuity and get a smooth function, SOC also needs to be transformed to the diabatic representation,

$$\begin{pmatrix} W_{0,p}^d \\ W_{1,p}^d \end{pmatrix} = \begin{pmatrix} \langle S_0^d | \mathrm{Hso} | T_{1,p} \rangle \\ \langle S_1^d | \mathrm{Hso} | T_{1,p} \rangle \end{pmatrix} = \begin{pmatrix} \cos\theta & -\sin\theta \\ \sin\theta & \cos\theta \end{pmatrix} \begin{pmatrix} \langle S_1^a | \mathrm{Hso} | T_{1,p} \rangle \\ \langle S_1^a | \mathrm{Hso} | T_{1,p} \rangle \end{pmatrix}. \tag{9}$$

Here, p = −, +, 0 and $W_{i,-}^d = X_i^d$, $W_{i,+}^d = Y_i^d$, and $W_{i,0}^d = Z_i^d$, see below, for time reversal adapted components of the triplet. While it is still possible to skip the diabatization step and use the adiabatic spin–orbit coupling term to do the dynamics calculation,[29,49] one can expect that approach to fail when a CI seam exists.

In the spin-diabatic representation, $\mathbf{H}_{tot}$ then has the following form:

$$\begin{array}{ccccccc} & |S_0\rangle & |S_1\rangle & |T_-\rangle & |T_+\rangle & |T_0\rangle \\ \langle S_0| & H_{11}^d & H_{12}^d & X_0^d & Y_0^d & Z_0^d \\ \langle S_1| & H_{21}^d & H_{22}^d & X_1^d & Y_1^d & Z_1^d \\ \langle T_-| & X_0^d & X_1^d & E_t & 0 & 0 \\ \langle T_+| & Y_0^d & Y_1^d & 0 & E_t & 0 \\ \langle T_0| & Z_0^d & Z_1^d & 0 & 0 & E_t \end{array} \tag{10}$$

The above matrix can be diagonalized to get the spin-adiabatic representation of the two singlets and one triplet system. Apart from a fixed eigenvalue $\lambda_3 = E_t$, it is challenging to determine explicit expressions for eigenvalues as the eigenequation is quartic. This partial solution is reported in Appendix B, with $\lambda_3 = E_t$ being a nondegenerate eigenvalue for the above matrix, which cannot form a CI with neighboring states. Note that this does not eliminate the existence of CIs for other paired states, roots (E_1,E_2) or (E_4,E_5). Here and below, we use (/) [(,)] to denote nonrelativistic (relativistic) intersections (or close approach).

B. The derivative coupling and its relation to the geometric phase

According to the GP theorem,[18,19,50] the real-valued wavefunction changes sign when traversing a loop that contains an odd number of CIs. Since it is more convenient to transport matrix elements than functions along such a path, it is useful to use an alternative signature of the geometric phase. As we show below, transporting the

derivative coupling along such a path provides the useful surrogate. To do this, define the following vectors whose origin is a CI:

$$\begin{aligned} \mathbf{h}^{IJ} &= \mathbf{d}^{I}\nabla_{R}\mathbf{H}_{s}\mathbf{d}^{J}, \\ 2\mathbf{g}^{IJ} &= (\mathbf{h}^{II} - \mathbf{h}^{JJ}), \\ 2\mathbf{s}^{IJ} &= (\mathbf{h}^{II} + \mathbf{h}^{JJ}). \end{aligned} \tag{11}$$

The **g**, **h** vectors are the well-known orthogonal intersection adapted coordinates that lift the degeneracy linearly near a CI.[51] Define the polar coordinate system (ρ, θ) originating at the CI as $\rho\cos\theta = gR_1$ and $\rho\sin\theta = hR_2$, where $||\mathbf{g}^{IJ}|| = g$ and $||\mathbf{h}^{IJ}|| = h$. The Hamiltonian for small **R** can then be written as

$$H(\mathbf{R}) = \begin{pmatrix} s(\mathbf{R}) - \mathbf{g}\mathbf{R}_1 & \mathbf{h}\mathbf{R}_2 \\ \mathbf{h}\mathbf{R}_2 & s(\mathbf{R}) + \mathbf{g}\mathbf{R}_1 \end{pmatrix}, \tag{12}$$

and the AtD transformation **d**(**R**) between states I and J is given by

$$\begin{pmatrix} \Psi_I^{(d)}(\mathbf{r};\mathbf{R}) \\ \Psi_J^{(d)}(\mathbf{r};\mathbf{R}) \end{pmatrix} = \begin{pmatrix} \cos\theta/2 & -\sin\theta/2 \\ \sin\theta/2 & \cos\theta/2 \end{pmatrix} \begin{pmatrix} \Psi_I^{(a)}(\mathbf{r};\mathbf{R}) \\ \Psi_J^{(a)}(\mathbf{r};\mathbf{R}) \end{pmatrix}. \tag{13}$$

Using Eqs. (3) and (13), one arrives at

$$\mathbf{f}_{IJ}^{a} = -\nabla_{\mathbf{R}}(\theta/2). \tag{14}$$

When θ increases from 0 to 2π, the line integral becomes the circulation, and we have

$$\oint \mathbf{f}^{I,J,CI}(\mathbf{R})\cdot d(\mathbf{R}) = \int_0^{2\pi}\frac{1}{2}d\theta = \pi. \tag{15}$$

To summarize, the circulation of the derivative coupling reflects the GP effect and, in turn, can be used to demonstrate the existence of a conical intersection as has been done by Baer.[46,47,52–55] Relations such as Eq. (15) are relevant in the construction of sub-Hilbert spaces.[1]

C. Locating seams

In the absence of an analytic formula for the eigenvalues of the Hamiltonian in Eq. (10), we turn to Lagrange multipliers (LMs) to locate the degeneracies, the CI seams. A geometry constrained Lagrange multiplier method is used to locate energy minimized crossings of state I and J = I ± 1 in the spin-adiabatic representation.[56,57] Here, I, I ± 1 can represent any of the spin-adiabatic eigenstates. The Lagrangian used in the optimization is defined as follows:

$$L^{IJ} = (E^{I} + E^{J})/2 + \lambda_1\Delta E^{IJ} + \lambda_2 H^{IJ} + \sum_{i=1}^{n_c}\kappa_i K_i. \tag{16}$$

Here, $\mathbf{K_i}$ corresponds to the i-th geometric constraint.

The constraints for the location of a conical intersection read

$$\begin{aligned} \mathbf{g}^{IJ}(R)\cdot\delta\mathbf{R} + \Delta E^{IJ} &= 0, \\ \mathbf{h}(\mathbf{R})\cdot\delta\mathbf{R} &= 0, \\ \nabla\mathbf{K}\cdot\delta\kappa + \mathbf{K} &= 0. \end{aligned} \tag{17}$$

The first two constraints (λ_1, λ_2) constrain the solution to be on the CI seam. A certain number of geometrical constraints **K** = 0 can be placed in the optimization. The average energy of the two states is minimized. It is then possible to get an energy minimized crossing in the spin-adiabatic representation by solving the following equation iteratively:

$$\begin{pmatrix} \nabla\nabla L & (\mathbf{g}) & (\mathbf{h}) & (\nabla\mathbf{K}) \\ (\mathbf{g})^{\dagger} & 0 & 0 & \\ (\mathbf{h})^{\dagger} & 0 & 0 & 0 \\ (\nabla K)^{\dagger} & 0 & & 0 \end{pmatrix} \begin{pmatrix} \delta\mathbf{R} \\ \delta\lambda_1 \\ \delta\lambda_2 \\ \delta\kappa \end{pmatrix} = -\begin{pmatrix} \nabla L \\ \Delta E^{IJ} \\ 0 \\ K \end{pmatrix}. \tag{18}$$

The first and second order gradient terms in Eq. (18) are evaluated by divided difference differentiation using the smooth analytic fit surfaces of $\mathbf{H}^{d}$ and SOC.

III. NUMERICAL EXAMPLE

We consider the three lowest states of NH_3, which are the two singlet (S_0,S_1) states and one triplet (T_1). A coupled diabatic state representation is required for the singlets, which exhibit a seam of conical intersection. An adiabatic representation of the triplet and the dipole, transition dipole, and spin–orbit coupling surfaces has been reported in a previous paper.[43] We summarize the results of that report below. The spin–orbit coupling matrix elements are scaled by a factor of 20 to emphasize their contributions while not disturbing their geometry dependence.

A. H_{sf} and H_{so} *ab initio* results and fit surface representations

The coupled potential energy surfaces and spin–orbit coupling surfaces sample 2956 *ab initio* points with a fitting rms error <10%. The neural network surfaces are used in the numerical calculations below and provide the diabatic Hamiltonian matrix of the two singlets, the energy of the triplet, and six SOC matrix elements between singlets and triplet. The energy and energy gradients of S_0, S_1, and T_1 and derivative coupling between S_0 and S_1 used in this work were obtained previously using multireference configuration interaction (MRCI) with all single- and double-excitation wavefunctions using the COLUMBUS program.[58] The basis set used is aug-cc-pVTZ with an extra Rydberg s-function on N(s, 0.028). The molecular orbitals are obtained from state-averaged multi-configuration self-consistent field (MCSCF) treatment that averages S_0, S_1, and T_1 with equal weights and a complete active space consisting of eight electrons in nine orbitals. The resulting MRCI expansion consists of 33 869 430 configuration interaction functions (CSFs) for the singlets and 59 141 259 CSFs for the triplet. The SOC matrix elements are calculated in the Breit–Pauli approximation and were obtained from the MOLPRO[59] MRCI with the same basis set and active space as that used in COLUMBUS.

B. Locating the seams (S_0,S_1,T_1)

Figure 1 plots the diagonal elements of the 5 × 5 spin-diabatic Hamiltonian matrix as a function of the N–H distance along a C_{2v} path. This plot in the spin-diabatic representation anticipates two crossings in the spin-adiabatic representation, the nonrelativistic (T_1/S_0) crossing that will become the (E_1,E_2) CI in the spin-adiabatic representation and the second crossing is (S_0/S_1) using H_{sf}, which will become the (E_4,E_5) CI in the spin-adiabatic representation. Figure 2 provides a detailed picture of the energies in the (S_0/S_1) CI region for C_{2v} geometries. Both spin-diabatic and spin-adiabatic representations are shown. In the latter representation, the triplets are no longer degenerate, and they can cross with the singlets in different places on the potential energy surfaces.

Using a point near the crossing as starting guess, we use the Lagrange multiplier (LM) method to locate (E_1,E_2) and (E_4,E_5), exact CIs with minimized energy in the full spin-adiabatic space. A typical search using the LM method is reported in Table I, which demonstrates the efficiency of the algorithm. The minimum energy crossing point energies are reported in Table II. One can see that although the separation of the singlet and triplet energies is only ~16 cm^{-1} in the Franck–Condon region according to Appendix C, it may lead to energy differences as much as hundreds of wavenumbers between the nonrelativistic CIs and those in spin-adiabatic representation. Moreover, running the search algorithm for (E_2,E_3) crossings and (E_3,E_4) crossing leads to nonconvergence. This is consistent with the analysis in Sec. II and Appendix B that state 3 does not cross with neighboring states.

We next turn to one of the key issues in this (and future) work, the differences between the nonrelativistic and relativistic CI seams. We initially focus on the g and h vectors. The g and h vectors for CIs (E_1,E_2) and (E_4,E_5) are plotted in Figs. 3 and 4, respectively. At the (E_4,E_5) crossing, the g and h vectors are similar to those of the nonrelativistic (S_0/S_1) CI reported in Ref. 60. Here, the S_0 and S_1 contributions to E_4 and E_5 are preeminent. On the other hand, the (E_1,E_2) crossing behaves differently from the (E_4,E_5) crossing as the h vector contains large contribution from the gradients of spin–orbit coupling. Furthermore, while (S_0/S_1) and (E_4,E_5) are true CIs (for different Hamiltonians), (S_0/T_1) is not, so an (S_0/T_1), (E_1/E_2) comparison is somewhat unfair. Detailed seams are plotted in Figs. 5 and 6. The CI points in the plots are LM energy minimized points with constraints on NH bond distance. From Fig. 5, the (S_0/S_1) CI seam is seen to be similar to the (E_4,E_5) seam in their geometry dependence but different in energy, which proves that state mixing is not obvious. Inclusion of SOC changes the energies of degenerate points. In Fig. 6, the pseudoseam (S_0/T_1) and (E_1,E_2) seam are juxtaposed. Differences are evident due to the strong triplet–singlet mixing in this region. Given that only the (E_1,E_2) seam has any interstate coupling (H_{so}), the inclusion of a geometry dependent SOC changes not only the energies but also their geometry dependence dramatically. This is consistent with the earlier g, h observations. For a background discussion of the geometry dependence of SOC matrix elements of NH_3, we refer the reader to Ref. 43.

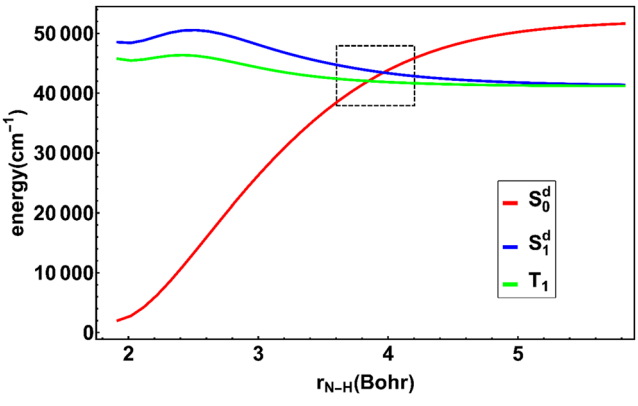

FIG. 1. Electronic energy of S_0, S_1, and T_1 plotted as a function of N–H distance.

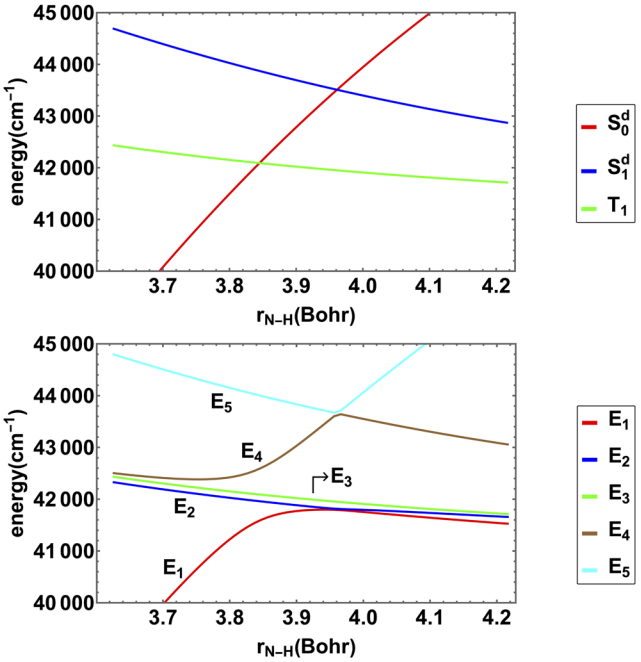

FIG. 2. Zoomed-in view of the rectangular selected region in Fig. 1: the upper panel denotes the spin-diabatic representation, and the bottom panel denotes the spin-adiabatic representation.

TABLE I. Convergence of a conical intersection search for an (E_1,E_2) CI a.b × 10^c is written as a.b(c).

Iterations	ΔE^{12}	$\|\|L\|\|$	E_1 (cm^{-1})	E_2 (cm^{-1})
0	1.0(−3)	9.0(−3)	40 443	40 672
1	5.6(−4)	4.3(−3)	40 378	40 501
2	3.6(−4)	2.7(−3)	40 348	40 426
3	2.2(−4)	1.7(−3)	40 320	40 369
4	1.3(−4)	5.9(−4)	40 311	40 339
5	5.9(−5)	9.8(−5)	40 313	40 326
6	2.4(−5)	6.3(−5)	40 315	40 320
7	7.7(−6)	3.4(−5)	40 318	40 319
8	3.2(−6)	7.1(−6)	40 320	40 320

TABLE II. Energy of CIs: $\text{minx}_{(1,2)}$ and $\text{minx}_{(4,5)}$. The intersections (S_0/T_1) and (S_0/S_1) are included for comparison with $\text{minx}_{(1,2)}$ and $\text{minx}_{(4,5)}$, respectively.

		E_1 (cm^{-1})	E_2 (cm^{-1})	E_3 (cm^{-1})	E_4 (cm^{-1})	E_5 (cm^{-1})
H_{tot}	minx(1,2)	40 320	40 320	40 440	42 367	42 707
	minx(4,5)	40 332	40 352	40 465	42 512	42 512
		S_0 (cm^{-1})	S_1 (cm^{-1})	$T_{1,+1}$ (cm^{-1})	$T_{1,-1}$ (cm^{-1})	$T_{1,0}$ (cm^{-1})
H_{sf}	minx(S_0/T_1)	40 675	42 787	40 675	40 675	40 675
	minx(S_0/S_1)	42 373	42 373	40 392	40 392	40 392

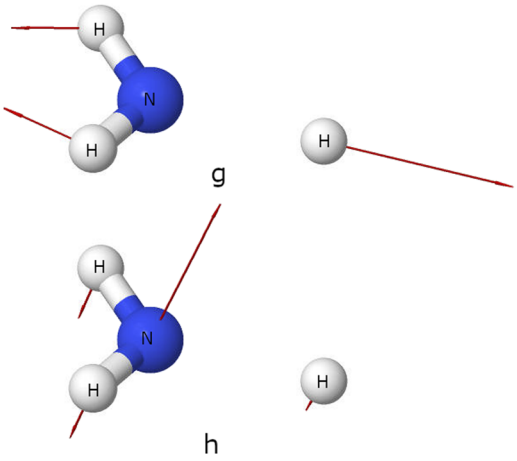

FIG. 3. g and h vector at minx(4,5) in the spin-adiabatic representation.

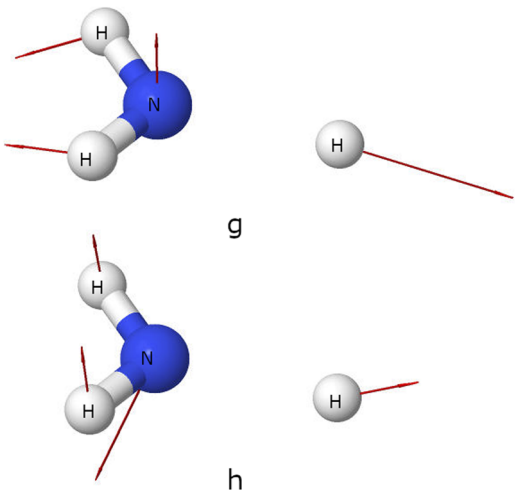

FIG. 4. g and h vector at minx(1,2) in the spin-adiabatic representation.

C. Geometric phase

The evaluation of the circulation of the derivative coupling, its line integral along a closed loop, is done by integrating the relativistic derivative coupling in the spin-adiabatic representation in the g–h plane in the polar coordinate system (ρ, θ) defined in Sec. II. The derivative coupling obtained using the analytic surface has an arbitrary phase as a consequence of the diagonalization. Such a problem can be avoided by computing the derivative coupling at θ and θ + dθ and comparing them to select the correct phase. When dθ is small enough, the evolution in the eigenvector is trivial and easy to

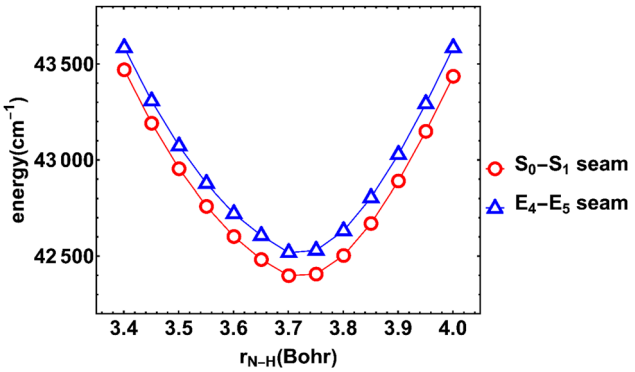

FIG. 5. The S_0–S_1 seam and E_4–E_5 seam plotted as a function of N–H distance.

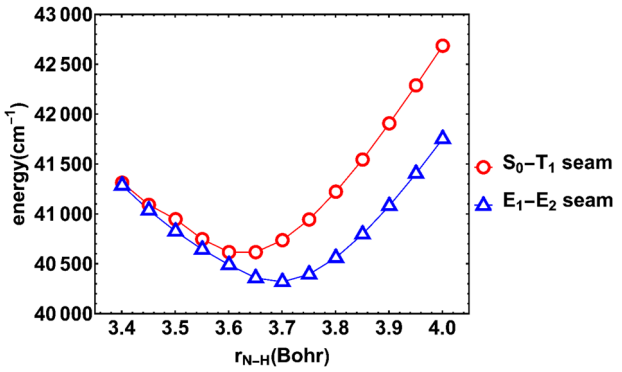

FIG. 6. The S_0–T_1 seam and E_1–E_2 seam plotted as a function of N–H distance.

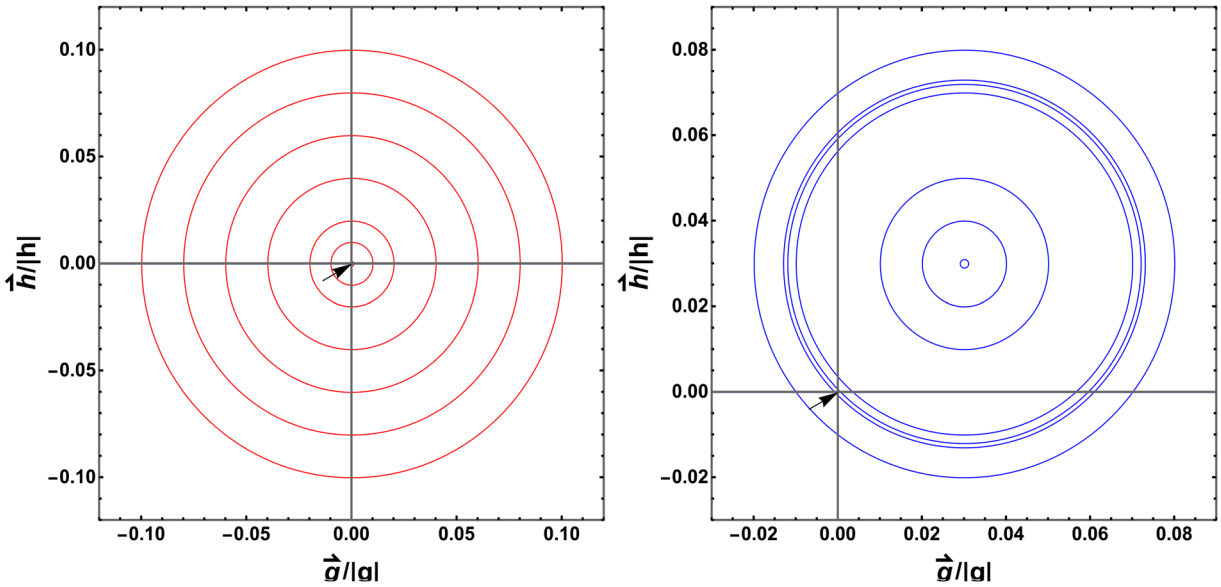

FIG. 7. The contour that is used to evaluate the circulations in Tables III and IV. CI between states 1 and 2 is placed at (0,0) and is marked with an arrow. Left panel: Table III. Right panel: Table IV.

distinguish from the one with the opposite sign. In all following calculations (which necessarily employed the fit surfaces), 10 000 steps are used in the evaluation of the circulation.

In an electronic Hamiltonian, the derivative coupling contains a nonremovable part when $N^{state} \geq 2$.[61] When $N^{state} = 2$, the (*ab initio*) derivative coupling may still contain a nonremovable part unless special care is taken.[15,62] These assertions are obtained by calculating the circulation of the derivative coupling placing the origin exactly at minx(E_1,E_2), minx(E_4,E_5), and minx(S_0/S_1) determined above with different radii, as shown in the left panel of Fig. 7. The results are reported in Table III. The circulation in the two-state representation is strictly π, while in a five-state representation, it deviates from π as ρ increases, a consequence of the dimension of the embedding space, as explained in Ref. 61. Thus, this method for proving the existence of conical intersection works best for small radii.

Next, we place the origin off the CI seam and increase ρ until a CI is captured, as in the right panel of Fig. 7. The line integral method can be used to verify the existence of a conical intersection. This can be useful especially when the position of a CI is unknown. Table IV shows the circulation when the loop radius increases from ρ = 0.042 to ρ = 0.043; the sudden increase in the circulation marks that the CI is suddenly included in the loop. Figure 8 plots $\mathbf{f}_\theta^{IJ}$, I = 1, J = 2, and the energies along the closed loop for ρ = 0.043 and ρ = 0.042. It can be seen from Fig. 8 that energy and the derivative coupling plot can both be misleading in determining the presence of CI, especially when the energy difference is small. In such a situation, $\mathbf{f}_\theta^{IJ}$ and its circulation are a better method, being sensitive to the CI's existence. Note that the circulation for ρ = 0.043 is ~0.1, which is again the nonremovable part. This value, however, can be larger when ρ increases. One should not let this affect the determination of the change in the circulation when using the line integral method.

We determine the circulation along a path that connects minx(E_1,E_2) and minx(E_4,E_5), as shown in Fig. 9. As has been mentioned above, states (E_2,E_3) and (E_3,E_4) do not form a CI. This is verified using the circulation plotted in the right panel

TABLE III. Circulation C(E_1,E_2), C(E_4,E_5), and C(S_0/S_1) with respect to radius ρ.

ρ	C(E_1,E_2)	C(E_4,E_5)	C(S_0/S_1)
0.0001	3.141 592	3.141 592	3.141 593
0.001	3.141 578	3.141 581	3.141 593
0.01	3.140 278	3.140 305	3.141 593
0.02	3.136 141	3.136 227	3.141 593
0.04	3.116 289	3.117 041	3.141 593
0.06	3.068 837	3.072 432	3.141 593
0.08	2.965 988	2.978 875	3.141 593
0.1	2.784 950	2.815 622	3.141 593

TABLE IV. Circulation for displaced loops C(E_1,E_2) with respect to radius ρ(dθ = 2π/10 000). Origin is placed slightly off the CI.

P	C
0.001	0.000 043 29
0.01	0.004 406
0.02	0.018 561
0.04	0.087 590
0.042	0.098 233
0.043	3.037 963
0.05	2.993 763

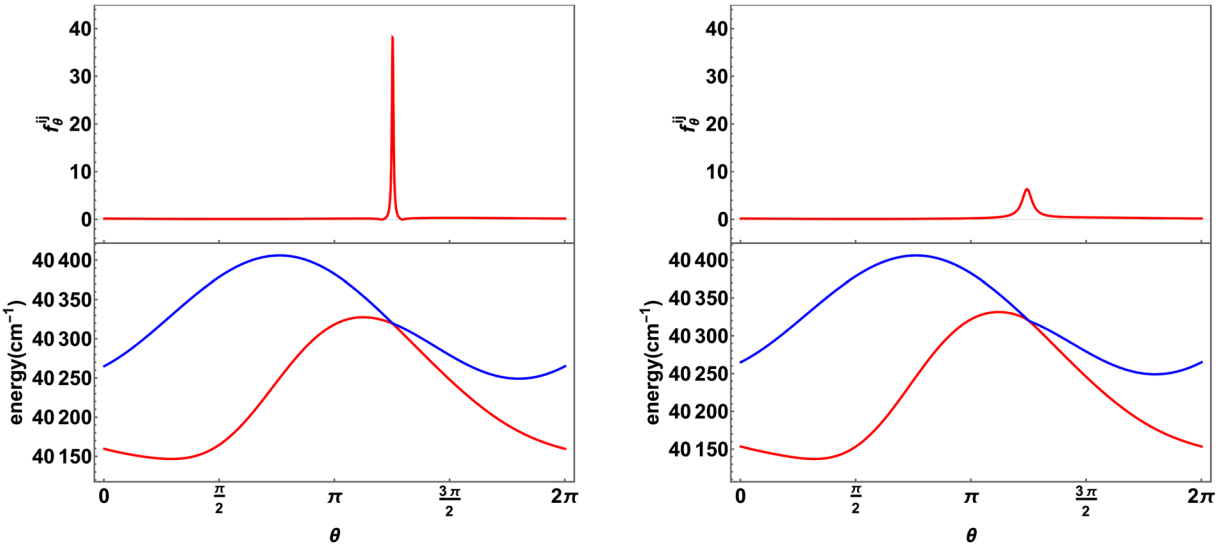

FIG. 8. f_θ^{ij} and energy as a function of θ. The left/right panel corresponds to ρ = 0.043/0.042 in Table IV.

of Fig. 9. The integral captures the CI of pair state (E_1,E_2) and (E_4,E_5) with desired accuracy (ρ = 0.001). The circulation for f^{23} and f^{34} remains near zero (~10^{-3}) along the path, even if we used a much large radius (ρ = 0.1). This is consistent with the nonexistence of minx(E_2,E_3) or minx(E_3,E_4) along or near the path.

The derivative coupling defined in the nonrelativistic case has been used in dynamics simulations to determine the hopping direction and probabilities between states with the same multiplicity. It would then be natural for one to think about employing the current nonrelativistic code with the minimum modification by treating the three components of triplets as individual states that can interact with other states. However, according to the analysis and numerical examples above, the CI can only exist between certain pair of states in such a system. Specifically, the derivative coupling between different components of triplet precludes any transition possibility between them. Thus, further modification may be needed in order to treat the triplet components correctly. Future work will focus on the dynamic simulation using current surfaces, accounting for the geometric phase of conical intersection in the spin-adiabatic representation and incorporating a correct treatment of singlet–triplet transition.

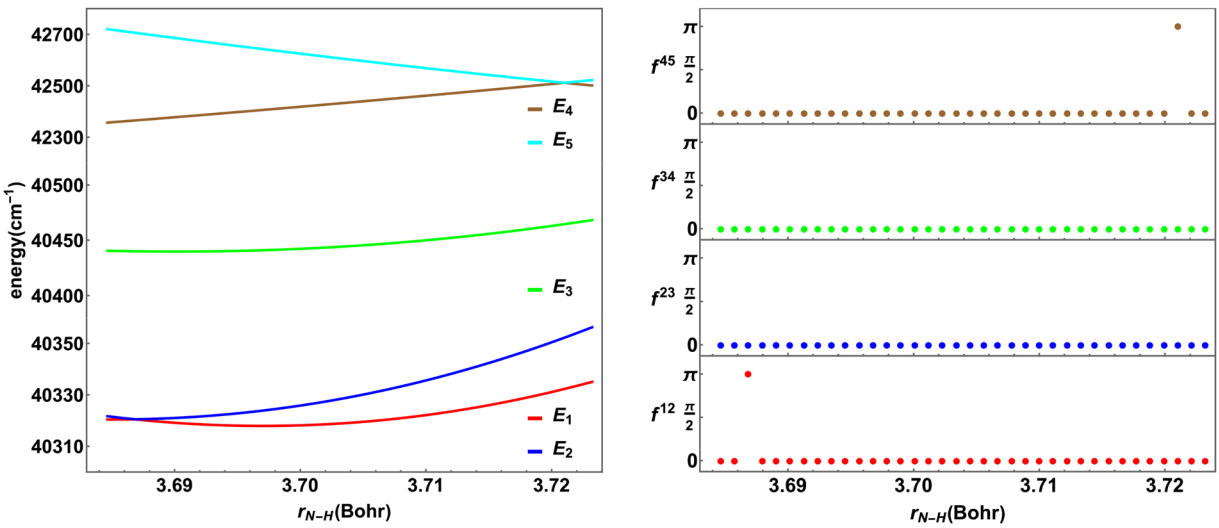

FIG. 9. Energy and circulation $\oint f^{ij} d\theta$ for points along the linear path connecting minx(1,2) and minx(4,5). Note that for illustration purpose, the tick on the y axis is not consistent.

IV. CONCLUSION

Conical intersections, derivative couplings, the geometric phase effect, and related quantities are studied for spin–orbit coupled systems using the spin-diabatic approximation with an even number of electrons. The relativistic wavefunctions are expanded in a spin-diabatic basis whose members are time reversal adapted. The use of time-reversal adapted bases for systems with even numbers of electrons makes the electronic Hamiltonian real-valued, greatly simplifying the analysis. We work in the Breit–Pauli approximation. In an elementary four state representation (one singlet and one triplet), one eigenvalue in the spin-adiabatic representation is always double-degenerate, and there is no conical intersection. In a frequently used five-state representation (two singlets, one triplet) readily generalized to *n* singlets, *m* triplets, conical intersections can only be formed at the (E_1,E_2) and (E_4,E_5) crossing. Formal results are juxtaposed with those of a numerical example, the $1,2^1A$ and 1^3A states of ammonia with an enhanced spin–orbit interaction. The geometric phase effect in the spin-adiabatic state representation is discussed and will be treated in future dynamics simulations.

ACKNOWLEDGMENTS

This work was supported by the U.S. National Science Foundation (Grant No. CHE-1954723 to D.R.Y.). The authors acknowledge the Maryland Advanced Research Computing Center (MARCC) at Johns Hopkins University and the National Energy Research Scientific Computing Center (NERSC) for computer time.

AUTHOR DECLARATIONS

Conflict of Interest

The authors have no conflicts to disclose.

DATA AVAILABILITY

The data that support the findings of this study are available within the article.

APPENDIX A: TIME REVERSAL SYMMETRY[63]

The time reversal operator (T) is singled out for special treatment since it is anti-unitary, that is, $T = UK$, where U is the unitary and K is the complex conjugation. T^2 has two outcomes: $T^2 = +1$ (even number of electrons) and $= -1$ (odd number of electrons). For an even number of electrons in the time reversal adapted basis, $T\psi_{j=}$ $j = 1, \ldots, N$, we can have

$$\psi_j = T\psi_j. \tag{A1}$$

Therefore, for an even number of electrons in a time reversal adapted basis where [T,H] = 0,

$$\begin{aligned} \langle\psi_i|H|\psi_j\rangle^* &= \langle T\psi_i|TH|\psi_j\rangle, \\ \langle T\psi_i|TH|\psi_j\rangle &= \langle T\psi_i|H|T\psi_j\rangle = \langle\psi_i|H|\psi_j\rangle, \end{aligned} \tag{A2}$$

and H is real-valued. To derive the results in Eq. (5), we illustrate for two electrons, where $\psi_+ \sim\alpha\alpha$, $\psi_- \sim\beta\beta$, and $\psi_{0\pm} \sim\alpha\beta \pm \beta\alpha$. T is given by $T = \sigma_y(1)\sigma_y(2)K$, where $\sigma_y = \begin{pmatrix} 0 & -i \\ i & 0 \end{pmatrix}$. Hence, for example, $T\alpha\alpha = \beta\beta$ and $T\alpha\beta = -\beta\alpha$, and it follows that the left-hand side of Eq. (5) in the main text is time reversal adapted.

APPENDIX B: THE FIXED EIGENVALUE IN (S_0,S_1,T_1) SYSTEM

Consider the symmetric matrix $\begin{pmatrix} a_{11} & a_{12} & x_1 & y_1 & z_1 \\ a_{12} & a_{22} & x_2 & y_2 & z_2 \\ x_1 & x_2 & a_{33} & 0 & 0 \\ y_1 & y_2 & 0 & a_{33} & 0 \\ z_1 & z_2 & 0 & 0 & a_{33} \end{pmatrix}$.

The eigenvalues are $\lambda_1 = a_{33}$, with λ_2, λ_3, λ_4, and λ_5 being the solution to a quartic equation.

The coefficients of the quartic equation are related to the solution of Eqs. (B1)–(B4), where

$$\lambda_2 + \lambda_3 + \lambda_4 + \lambda_5 = a_{11} + a_{22} + 2a_{33}, \tag{B1}$$

$$\begin{aligned} &\lambda_2\lambda_3 + \lambda_2\lambda_4 + \lambda_2\lambda_5 + \lambda_3\lambda_4 + \lambda_3\lambda_5 + \lambda_4\lambda_5 \\ &\quad = -a_{12}^2 + a_{11}a_{22} + 2a_{11}a_{33} + 2a_{22}a_{33} \\ &\qquad + a_{33}^2 - x_1^2 - x_2^2 - y_1^2 - y_2^2 - z_1^2 - z_2^2, \end{aligned} \tag{B2}$$

$$\begin{aligned} &\lambda_2\lambda_3\lambda_4 + \lambda_2\lambda_3\lambda_5 + \lambda_2\lambda_4\lambda_5 + \lambda_3\lambda_4\lambda_5 \\ &\quad = -2a_{12}^2a_{33} + 2a_{11}a_{22}a_{33} + a_{11}a_{33}^2 + a_{22}a_{33}^2 - a_{22}x_1^2 \\ &\qquad - a_{33}x_1^2 + 2a_{12}x_1x_2 - a_{11}x_2^2 \\ &\qquad - a_{33}x_2^2 - a_{22}y_1^2 - a_{33}y_1^2 + 2a_{12}y_1y_2 - a_{11}y_2^2 - a_{33}y_2^2 \\ &\qquad - a_{22}z_1^2 - a_{33}z_1^2 + 2a_{12}z_1z_2 - a_{11}z_2^2 - a_{33}z_2^2, \end{aligned} \tag{B3}$$

$$\begin{aligned} \lambda_2\lambda_3\lambda_4\lambda_5 = &- a_{12}^2a_{33}^2 + a_{11}a_{22}a_{33}^2 - a_{22}a_{33}x_1^2 + 2a_{12}a_{33}x_1x_2 \\ &- a_{11}a_{33}x_2^2 - a_{22}a_{33}y_1^2 + x_2^2y_1^2 + 2a_{12}a_{33}y_1y_2 \\ &- 2x_1x_2y_1y_2 - a_{11}a_{33}y_2^2 + x_1^2y_2^2 - a_{22}a_{33}z_1^2 + x_2^2z_1^2 \\ &+ y_2^2z_1^2 + 2a_{12}a_{33}z_1z_2 - 2x_1x_2z_1z_2 - 2y_1y_2z_1z_2 \\ &- a_{11}a_{33}z_2^2 + x_1^2z_2^2 + y_1^2z_2^2. \end{aligned} \tag{B4}$$

Let $\lambda_2 = a_{33}$. Substituting into (B1), we have

$$\lambda_3 + \lambda_4 + \lambda_5 = a_{11} + a_{22} + a_{33}. \tag{B5}$$

Simplifying Eq. (B4) − a_{33}* [(B3) − ((B2) − a_{33}* (B5))] and using $\lambda_2 = a_{33}$, we obtain $(x_1y_2 - x_2y_1)^2 + (y_2z_1 - y_1z_2)^2 + (x_1z_2 - x_2z_1)^2 = 0$.

Note that the equation holds only when $x_1y_2 = x_2y_1$, $x_1z_2 = x_2z_1$, and $y_1z_2 = y_2z_1$ are satisfied simultaneously. Although this can be achieved in theory, one would expect that in practical problem, the SOC vector from different singlets with the triplet cannot be linear dependent. It contradicts with the assumption that $\lambda_2 = a_{33}$, and thus, $\lambda_1 = a_{33}$ is a unique eigenvalue of the symmetric matrix above.

APPENDIX C: ENERGY SPLITTING IN SPIN-ADIABATIC REPRESENTATION

As has been noted above, the eigenvalues in the (S_0,S_1,T_1) system cannot be written down analytically. However, it is still necessary to present the actual effect of spin–orbit coupling on the energy

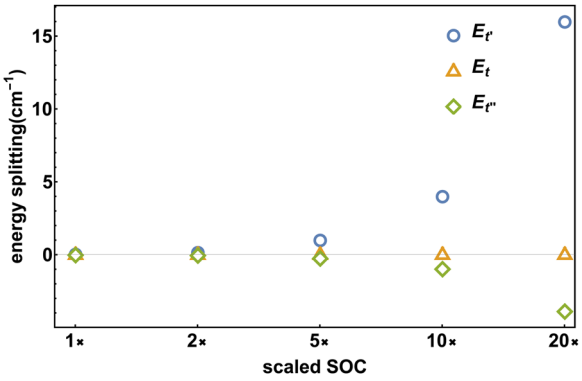

FIG. 10. Energy splitting as a function of the scaled SOC.

splitting of triplets. Figure 10 shows the triplets splitting relative to E_t. The point showed in the plot is the S_1 minimum, which is in the Frank–Condon region. The reason for choosing points in the Frank–Condon region is that the state mixing is limited. From Fig. 10, the splitting becomes larger when the absolute value of spin–orbit coupling increases. This is not surprising as the triplets itself do not couple with other triplets, and the splitting can only be controlled through their coupling with singlets. For ammonia, one may expect that the splitting is small as its spin–orbit coupling is only around 15 cm^{-1}. However, when the spin–orbit coupling is scaled by factor of 20, the splitting cannot be overlooked. It is also expected that the splitting will increase with increased state mixing, for example, near singlet–triplet crossing or conical intersection. Under such circumstances, the energy splitting has to be taken into account.

In practical problems, one may expect that the SOC in one direction is significantly larger than other components. This feature has been used to simplify the cluster growing algorithm to select the correct phase of spin–orbit coupling.[35,43] The relative splitting can be manipulated with the dominate component(s), as shown in Fig. 11. When the SOC matrix elements in one singlet state with the triplet dominates (examples 1, 2, 3 in Fig. 11), the splitting will be focused on one triplet component and the other two triplet components are

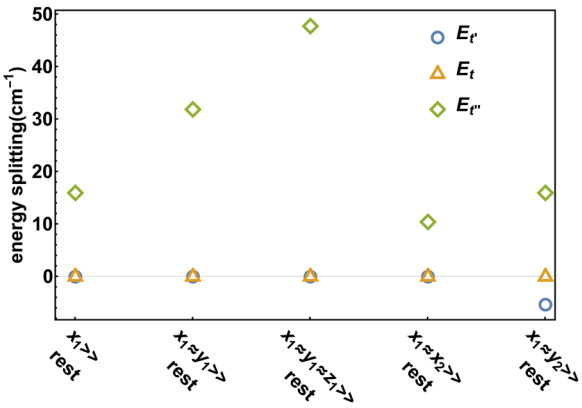

FIG. 11. Energy splitting due to different dominate components in the SOC matrix element. From left to right, five examples are shown. Here, rest means any component left in (x_1, y_1, z_1, x_2, y_2, z_2).

almost degenerate. This can be viewed as an approximation to the four-state case where the eigenvalues are strictly doubly degenerate. In order to have a relatively large splitting on both triplet components, one requires that the SOC matrix element between different triplet components and different singlets is comparable, for example, the last example in Fig. 11 when $x_1 \approx y_2 \gg$ the rest of SOC matrix elements. For better illustration, our discussion in this work will use the SOC that is scaled 20 times, as in Fig. 10. It should be pointed out that when scaled 20 times, the SOC is around 300 cm^{-1}, which is a reasonable value.

REFERENCES

[1] W. Domcke, D. R. Yarkony, and H. Köppel, *Conical Intersections: Electronic Structure, Dynamics and Spectroscopy* (World Scientific, Singapore, 2004).
[2] D. R. Yarkony, Rev. Mod. Phys. **68**, 985 (1996).
[3] W. Domcke, D. R. Yarkony, and H. Köppel, *Conical Intersections: Theory, Computation, and Experiment* (World Scientific, Singapore, 2011).
[4] M. Baer, *Beyond Born-Oppenheimer: Electronic Nonadiabatic Coupling Terms and Conical Intersections* (Wiley, NJ, 2006).
[5] A. W. Jasper, S. Nangia, C. Zhu, and D. G. Truhlar, Acc. Chem. Res. **39**, 101 (2006).
[6] S. Matsika and P. Krause, Annu. Rev. Phys. Chem. **62**, 621 (2011).
[7] J. E. Subotnik, E. C. Alguire, Q. Ou, B. R. Landry, and S. Fatehi, Acc. Chem. Res. **48**, 1340 (2015).
[8] B. G. Levine and T. J. Martínez, Annu. Rev. Phys. Chem. **58**, 613 (2007).
[9] F. Bernardi, M. Olivucci, and M. A. Robb, Chem. Soc. Rev. **25**, 321 (1996).
[10] H. Guo and D. R. Yarkony, Phys. Chem. Chem. Phys. **18**, 26335 (2016).
[11] S. Mai, P. Marquetand, and L. González, Wiley Interdiscip. Rev.: Comput. Mol. Sci. **8**, e1370 (2018).
[12] B. F. E. Curchod, C. Rauer, P. Marquetand, L. González, and T. J. Martínez, J. Chem. Phys. **144**, 101102 (2016).
[13] M. Barbatti, G. Granucci, M. Persico, M. Ruckenbauer, M. Vazdar, M. Eckert-Maksić, and H. Lischka, J. Photochem. Photobiol., A **190**, 228 (2007).
[14] K. A. Parker and D. G. Truhlar, J. Chem. Phys. **152**, 244309 (2020).
[15] J. Dutta, S. Mukherjee, K. Naskar, S. Ghosh, B. Mukherjee, S. Ravi, and S. Adhikari, Phys. Chem. Chem. Phys. **22**, 27496 (2020).
[16] T. Lenzen, W. Eisfeld, and U. Manthe, J. Chem. Phys. **150**, 244115 (2019).
[17] G. Herzberg and H. C. Longuet-Higgins, Discuss. Faraday Soc. **35**, 77 (1963).
[18] C. A. Mead and D. G. Truhlar, J. Chem. Phys. **70**, 2284 (1979).
[19] M. V. Berry, Proc. R. Soc. London, Ser. A **392**, 45 (1984).
[20] D. R. Yarkony, C. Xie, X. Zhu, Y. Wang, C. L. Malbon, and H. Guo, Comput. Theor. Chem. **1152**, 41 (2019).
[21] M. Abe, Y. Ohtsuki, Y. Fujimura, Z. Lan, and W. Domcke, J. Chem. Phys. **124**, 224316 (2006).
[22] B. K. Kendrick, J. Phys. Chem. A **107**, 6739 (2003).
[23] I. G. Ryabinkin, L. Joubert-Doriol, and A. F. Izmaylov, J. Chem. Phys. **140**, 214116 (2014).
[24] M. G. D. Nix, A. L. Devine, R. N. Dixon, and M. N. R. Ashfold, Chem. Phys. Lett. **463**, 305 (2008).
[25] C. Xie, C. L. Malbon, D. R. Yarkony, D. Xie, and H. Guo, J. Am. Chem. Soc. **140**, 1986 (2018).
[26] S. Mai, P. Marquetand, and L. González, Int. J. Quantum Chem. **115**, 1215 (2015).
[27] G. Cui and W. Thiel, J. Chem. Phys. **141**, 124101 (2014).
[28] F. An, J. Chen, X. Hu, H. Guo, and D. Xie, J. Phys. Chem. Lett. **11**, 4768 (2020).
[29] J. Westermayr, M. Gastegger, and P. Marquetand, J. Phys. Chem. Lett. **11**, 3828 (2020).
[30] L. Zhang, Y. Shu, S. Sun, and D. G. Truhlar, J. Chem. Phys. **154**, 094310 (2021).
[31] C. M. Marian, Wiley Interdiscip. Rev.: Comput. Mol. Sci. **2**, 187 (2012).
[32] C. M. Marian, Annu. Rev. Phys. Chem. **72**, 617 (2021).

[33]S. Mukherjee, D. A. Fedorov, and S. A. Varganov, Annu. Rev. Phys. Chem. **72**, 515 (2021).
[34]Y. Guan, H. Guo, and D. R. Yarkony, J. Chem. Theory Comput. **16**, 302 (2019).
[35]Y. Guan and D. R. Yarkony, J. Phys. Chem. Lett. **11**, 1848 (2020).
[36]C. A. Mead and D. G. Truhlar, J. Chem. Phys. **77**, 6090 (1982).
[37]J. Behler, Phys. Chem. Chem. Phys. **13**, 17930 (2011).
[38]B. J. Braams and J. M. Bowman, Int. Rev. Phys. Chem. **28**, 577 (2009).
[39]K. Shao, J. Chen, Z. Zhao, and D. H. Zhang, J. Chem. Phys. **145**, 071101 (2016).
[40]H. A. Bethe and E. E. Salpeter, *Quantum Mechanics of One- and Two-Electron Atoms* (Springer; Academic Press, Berlin, New York, 1957).
[41]S. R. Langhoff and C. W. Kern, Mod. Theor. Chem. **4**, 381 (1977).
[42]C. A. Mead, J. Chem. Phys. **70**, 2276 (1979).
[43]Y. Wang, Y. Guan, H. Guo, and D. R. Yarkony, J. Chem. Phys. **154**, 094121 (2021).
[44]G. Granucci, M. Persico, and G. Spighi, J. Chem. Phys. **137**, 22A501 (2012).
[45]M. Baer, J. Phys. Chem. A **104**, 3181 (2000).
[46]R. Baer, D. M. Charutz, R. Kosloff, and M. Baer, J. Chem. Phys. **105**, 9141 (1996).
[47]Z. Xu, M. Baer, and A. J. C. Varandas, J. Chem. Phys. **112**, 2746 (2000).
[48]M. Dallos, H. Lischka, R. Shepard, D. R. Yarkony, and P. G. Szalay, J. Chem. Phys. **120**, 7330 (2004).
[49]J. Westermayr and P. Marquetand, Chem. Rev. **121**, 9873 (2021).
[50]H. C. Longuet-Higgins, U. Öpik, M. H. L. Pryce, and R. A. Sack, Proc. R. Soc. London, Ser. A **244**, 1 (1958).
[51]D. R. Yarkony, J. Chem. Phys. **105**, 10456 (1996).
[52]M. Baer, J. Chem. Phys. **107**, 2694 (1997).
[53]M. Baer, Phys. Rep. **358**, 75 (2002).
[54]B. Esry and H. Sadeghpour, Phys. Rev. A **68**, 042706 (2003).
[55]G. W. Richings and G. A. Worth, J. Phys. Chem. A **119**, 12457 (2015).
[56]M. R. Manaa and D. R. Yarkony, J. Chem. Phys. **99**, 5251 (1993).
[57]Y. Wang and D. R. Yarkony, J. Chem. Phys. **149**, 154108 (2018).
[58]H. Lischka, T. Müller, P. G. Szalay, I. Shavitt, R. M. Pitzer, and R. Shepard, Wiley Interdiscip. Rev.: Comput. Mol. Sci. **1**, 191 (2011).
[59]H.-J. Werner *et al.*, MOLPRO, version 2012.1, a package of *ab initio* programs, 2012, see http://www.molpro.net.
[60]X. Zhu and D. R. Yarkony, Mol. Phys. **108**, 2611 (2010).
[61]C. L. Malbon, X. Zhu, H. Guo, and D. R. Yarkony, J. Chem. Phys. **145**, 234111 (2016).
[62]S. Mukherjee, S. Ravi, K. Naskar, S. Sardar, and S. Adhikari, J. Chem. Phys. **154**, 094306 (2021).
[63]M. Tinkham, *Group Theory and Quantum Mechanics* (McGraw-Hill, 1964), pp. 141–147.